ELSEVIER

Neurobiology of Aging 33 (2012) 2533–2550

NEUROBIOLOGY OF AGING

www.elsevier.com/locate/neuaging

Regular papers

Resting metabolic connectivity in prodromal Alzheimer's disease. A European Alzheimer Disease Consortium (EADC) project

Silvia Morbelli[a,*], Alex Drzezga[b], Robert Perneczky[c], Giovanni B. Frisoni[d], Anna Caroli[d,e], Bart N.M. van Berckel[f], Rik Ossenkoppele[f], Eric Guedj[g], Mira Didic[h], Andrea Brugnolo[i], Gianmario Sambuceti[a], Marco Pagani[j,k], Eric Salmon[l], Flavio Nobili[i]

[a] *Nuclear Medicine Unit, Department of Internal Medicine, San Martino University Hospital, Genoa, Italy*
[b] *Department of Nuclear Medicine, Technische Universität München, Munich, Germany*
[c] *Department of Psychiatry and Psychotherapy, Technische Universität München, Munich, Germany*
[d] *LENITEM Laboratory of Epidemiology and Neuroimaging - IRCCS S. Giovanni di Dio-FBF, Brescia, Italy*
[e] *Medical Imaging Unit, Biomedical Engineering Department, Mario Negri Institute for Pharmacological Research, Bergamo, Italy*
[f] *Department of Nuclear Medicine and PET Research, VU University Medical Center, Amsterdam, the Netherlands*
[g] *Service Central de Biophysique et de Médecine Nucléaire and Centre Européen de Recherche en Imagerie Médicale (CERIMED), Assistance Publique des Hôpitaux de Marseille, Faculté de Médecine, Université de la Méditerranée, INSERM, Marseille, France*
[h] *Service de Neurologie et de Neuropsychologie, Pôle de neurosciences cliniques, Assistance Publique des Hôpitaux de Marseille, Hôpitaux de la Timone, INSERM U751, Faculté de Médecine, Université de la Méditerranée, Marseille, France*
[i] *Clinical Neurophysiology Unit, Department of Neuroscience, Ophthalmology and Genetics, San Martino University Hospital, Genoa, Italy*
[j] *Institute of Cognitive Sciences and Technologies, CNR, Rome, Italy*
[k] *Department of Nuclear Medicine, Karolinska Hospital, Stockholm, Sweden*
[l] *Cognitive and Behavioral Neuroscience Centre, University of Liège, Liège, Belgium*

Received 10 September 2011; received in revised form 9 January 2012; accepted 12 January 2012

Abstract

We explored resting-state metabolic connectivity in prodromal Alzheimer's disease (pAD) patients and in healthy controls (CTR), through a voxel-wise interregional correlation analysis of 18F-fluorodeoxyglucose (FDG)-positron emission tomography (PET) by means of statistical parametric mapping. Baseline 18F-fluorodeoxyglucose-positron emission tomography of 36 patients with amnestic mild cognitive impairment who converted to Alzheimer's disease (AD) dementia after an average time of 2 years (pAD) and of 105 CTR were processed. The area of hypometabolism in pAD showed less metabolic connectivity in patients than in CTR (autocorrelation and correlation with large temporal and frontal areas, respectively). pAD patients showed limited correlation even in selected nonhypometabolic areas, including the hippocampi and the dorsolateral prefrontal cortex (DLFC). On the contrary, in CTR group correlation was highlighted between hippocampi and precuneus/posterior cingulate and frontal cortex, and between dorsolateral prefrontal cortex and caudate nuclei and parietal cortex. The reduced metabolic connections both in hypometabolic and nonhypometabolic areas in pAD patients suggest that metabolic disconnection (reflecting early diaschisis) may antedate remote hypometabolism (early sign of synaptic degeneration).

Keywords: Prodromal Alzheimer's disease; Positron emission tomography; Functional connectivity

1. Introduction

The human brain is anatomically and functionally organized into complex networks allowing both segregation and integration of information. Multidisciplinary research in neuroimaging has provided methods capable of exploring in

* Corresponding author at: Nuclear Medicine Unit, San Martino University Hospital, Largo R. Benzi 10, 16132 Genoa, Italy. Tel.: +39 0105552029; fax: +39 0105556911.
E-mail address: silviadaniela.morbelli@hsanmartino.it (S. Morbelli).

0197-4580/$ – see front matter © 2012 Elsevier Inc. All rights reserved.
10.1016/j.neurobiolaging.2012.01.005

vivo and noninvasively functional connectivity of these networks at the macroscopic level during task performance, both in healthy subjects and in several pathological conditions (Bressler and Menon, 2010). In addition, in the last decade functional connectivity has also been investigated during the task-free ("resting-state") condition, able to disclose a multiple interacting system called "default mode network" (DMN). This network would be mainly active at rest when individuals are engaged in internally focused tasks, including memory retrieval, future visualization, and conceiving the perspectives of others (Buckner et al., 2008; Raichle et al., 2001). The DMN includes medial prefrontal cortex, posterior cingulate and inferior parietal lobule, and can be identified through different neuroimaging methods. The most frequently used are task-free functional magnetic resonance imaging (fMRI) and regional cerebral blood flow (rCBF)-positron emission tomography (PET) which are based upon the detection of interregional correlations in spontaneous blood oxygen level-dependent (BOLD) signal fluctuations (Biswal et al., 1995) and resting state specific perfusion patterns, respectively (Beason-Held et al., 2009).

On the other hand, brain 18F-fluorodeoxyglucose (FDG)-PET is an effective method for investigating brain activity through observing changes in cerebral glucose metabolism, which essentially reflects synaptic glutamatergic activity (Salmon et al., 2009; Sestini et al., 2010). In the 1980s and 1990s, prior to the statistical parametric mapping (SPM) approach, a few studies (Horwitz et al., 1987, 1988, 1990, 1991) investigated the meaning of resting state intercorrelations of glucose metabolic rates between brain regions using a volume of interest (VOI) approach in healthy subjects, patients with Down's syndrome, autism, obsessive-compulsive disorder, and Alzheimer's disease (AD).

The basic assumptions are that brain regions whose metabolic levels are significantly correlated are functionally interconnected and that the strength of the connection is proportional to the magnitude of the correlation coefficient (Horwitz et al., 1984). This principle has been applied to show reduced functional connections of entorhinal cortex in AD patients at the stage of dementia, in comparison with healthy controls by using SPM (Mosconi et al., 2004b). This SPM approach has been more recently refined by Lee et al. (2008) who systematically explored metabolic connectivity based on voxel-wise interregional correlation analysis (IRCA) of SPM in normal healthy adults, thus establishing normative data of interregional metabolic connectivity. Given the consistency of resting-state networks across healthy subjects (Damoiseaux et al., 2006) this method could be used to disclose abnormalities of default metabolic connectivity in pathologic conditions.

Brain FDG-PET has shown a fairly good sensitivity in the early diagnosis of AD and is one of the currently accepted imaging biomarkers (Nestor et al., 2004; Nobili et al., 2008; Salmon et al., 2009). On the other hand resting functional connectivity, as assessed by means of both task-free fMRI and rCBF-PET studies, has revealed altered patterns of deactivation in AD (Bookheimer et al., 2000; Drzezga et al., 2005). Given the sequential coupling of neuronal activity, metabolism, and perfusion, regional metabolic connections might precede those concerning rCBF connections (rCBF-PET, fMRI) thus being further and earlier sensitive to the disease-induced alterations of brain function in the very early stage of AD. In the present study we aimed to explore resting metabolic connectivity in AD patients who underwent brain FDG PET when they were still at the stage of amnestic mild cognitive impairment (aMCI) in comparison with aged-matched healthy controls.

2. Methods

2.1. Subjects

The FDG-PET project of the European Alzheimer's Disease Consortium (EADC) (www.eadc.info) is aimed at joining together FDG-PET scans with corresponding clinical and neuropsychological data from patients with mild cognitive impairment (MCI) and normal controls from EADC centers. To date, 5 centers in 4 countries (namely, Amsterdam, Brescia, Genoa, Marseille, Munich) participate.

Patients with aMCI with or without impairment in other cognitive domains and healthy controls have been enrolled. As for aMCI, the inclusion criteria basically included outpatients newly referred for cognitive complaints to a center dedicated to the evaluation of cognitive disorders. All referrals were considered, including self- or relative-referral, referral from general practitioners, and from first-level neurological or geriatric clinics. Cognitive complaints mainly included memory complaints but they could also include difficulties in other cognitive domains, such as attention and orientation. Exclusion criteria were dementia; any somatic, metabolic (e.g., vitamin deficiency, endocrine untreated disorders, kidney, liver, or heart failure), psychiatric, or neurological disorder that may cause cognitive impairment, i.e., cerebrovascular accidents; neurodegenerative diseases, such as Parkinson's disease; severe head trauma; brain tumor; history of alcohol abuse; and severe depression. Dementia was excluded by the clinical interviews with patients and caregivers that excluded significant impairment in activities of daily living and by means of the Clinical Dementia Rating (CDR) scale (Hughes et al., 1982), scoring 0.5 in all aMCI patients. General cognition was assessed by means of the Mini Mental State Examination (MMSE) in all centers.

All subjects underwent rating scales for depression and neuropsychiatric symptoms according to the routine in use in each center. Patients with major depression, delusions, or hallucinations were excluded. Structural neuroimaging (mainly magnetic resonance imaging; MRI) was available; computed tomography (CT) was performed when MRI was unfeasible because of contraindications or patient intolerance.

Neuropsychological tests were administered in the domains of memory, language, executive function, attention, and visuoconstruction, according to the routine of each center, in order to define the aMCI syndrome, according to the Petersen's criteria (Petersen, 2004). Raw scores were converted to age-, education-, and gender-corrected *Z*-scores according to locally collected or normative data in use in each center that vary among countries and languages. Impairment was defined as a *Z*-score of −1.5 or lower. Subjects with impairment in the memory domain only (single-domain aMCI) or with impairment in the memory domain plus impairment in nonmemory domains (multidomain aMCI) were defined as aMCI.

Healthy controls accepted to participate as volunteers and were selected with the only criteria to be in the same age range of patients. They were judged to be in good health by general medical and neurological examinations, routine blood, and urine assays. Mild and well-controlled medical conditions, such as hypertension and diabetes, and a mild depressive trait were not considered as exclusion criteria. Only subjects not taking neuropsychoactive drugs or drugs known to interfere with cerebral metabolism were accepted in the control (CTR) group. Cognitive health was established in each center by means of the same interview and test battery in use for aMCI patients. Only subjects with an MMSE score $>$ 26 and a Clinical Dementia Rating $=$ 0 were included.

MCI patients were then regularly followed-up to pick up those developing dementia. During the follow-up, patients were carefully treated for systemic comorbidity; drugs known to depress brain synaptic transmission, such as benzodiazepines and tricyclic antidepressant, were slowly tapered and then withdrawn, when possible. None of the patients was taking antidementia medication at the time of either PET scan or during the follow-up period, until a formal diagnosis of AD-dementia was made. The study was approved by the local Medical Ethics Committee in each center and all the recruited subjects provided written informed consent.

The present work concerns data of subjects uploaded until September 2009. Brain FDG-PET of 109 patients with aMCI and 105 normal controls were available.

Each center had to upload a similar number of patients and controls in order to balance for the impact of different scanners among centers. Subject information and scans uploaded by each center were as follows: Brescia, 36 aMCI patients and 27 controls; Genoa, 31 aMCI patients and 33 controls; Munich, 23 aMCI patients and 19 controls; Amsterdam, 14 aMCI patients and 16 controls; and Marseille, 5 aMCI patients and 10 controls.

During a mean follow-up time of approximately 2 years, 36 out of the 109 aMCI patients progressed to AD dementia (from now on: "prodromal AD" patients, pAD: 18 men; mean age: 72.1 ± 8.4 years; mean baseline MMSE score: 27.5 ± 1.4; mean follow-up time: 24.6 ± 18.5 months). Diagnosis of dementia of the AD type was established according to the National Institute of Neurological and Communicative Disorders, Stroke, Alzheimer's Disease and Related Disorders Association (NINCDS-ADRDA) criteria (McKhann et al., 1984) and to the Diagnostic and Statistical Manual of Mental Disorders (DSM-IV R) criteria. The remaining 73 aMCI patients did not progress to dementia, but remained in the aMCI stage or reverted to normal condition during the follow-up (24 men; mean age: 73 ± 7.3 years; mean baseline MMSE score: 28.0 ± 1.8; mean follow-up time: 22.3 ± 15.9 months). Because of the possible statistical effect of the number unbalanced between pAD (n = 36) and CTR (n = 105), we selected a group of 36 CTR subjects (36 CTR) to compare with pAD patients, adopting a case-control procedure that took into consideration age, gender, and center of data acquisition. The same analysis was then repeated in the remaining 69 CTR (69 CTR) subjects serving as an independent control group to verify whether the findings obtained in the group of 36 CTR could be consistently replicated.

Table 1 reports the main baseline demographic characteristics of pAD and both 36 CTR and 69 CTR groups as well as their baseline and follow up MMSE scores.

2.2. PET procedures

FDG-PET was performed within 2 months from the baseline clinical-neuropsychological examination according to the European Association of Nuclear Medicine (EANM) guidelines (Bartenstein et al., 2002). Subjects fasted for at least 6 hours. Before radiopharmaceutical injection, blood glucose was checked and was $<$ 140 mg/dL in all subjects. Subjects were injected with 185–250 MBq of 18F-FDG via a venous cannula. Required minimum time interval between injection and scan start was 30 minutes. Required minimum scan duration was 10 minutes. Emission scans were acquired in 3-dimensional mode. Images were reconstructed

Table 1
Main baseline demographic and clinical characteristics of the 3 groups

Group	*n*	Age, y	Gender, M:F	Education, y	Follow-up time, mo	Baseline MMSE	Follow-up MMSE
Normal control subjects	69	68.7 ± 6.4	33:36	11.4 ± 3.9	13.3 ± 5.9	29.7 ± 0.8	29.4 ± 0.7
Normal control subjects	36	70.7 ± 6.5	19:17	11.7 ± 4.1	9.3 ± 3.8	29.3 ± 1	28.9 ± 1.5
Prodromal AD	36	72.1 ± 8.4	18:18	10.4 ± 4.2	24.6 ± 18.5	27.5 ± 1.4	23.9 ± 2.4

AD, Alzheimer's disease; F, female; M, male; MMSE, Mini Mental State Examination.

Table 2
Overview of participating centers and equipment

EADC center	Scanner type (manufacturer)	Spatial resolution		Axial field of view (mm)
		In-plane FWHM	Slick thickness	
Amsterdam	ECAT EXACT HR+ (1)	7.00	2.50	155
Brescia	Discovery ST (2)	5.99	2.34	157
Marseille	Discovery ST (2)	6.20	3.27	157
Genoa	Biograph Hi-rez (1)	5.80	3.75	162
Munich	ECAT EXACT HR+ (1)	7.00	2.46	155

EADC, European Alzheimer Disease Consortium; FWHM, full width at half maximum. Note. (1) Siemens, Munich, Germany; (2) GE Healthcare, Little Chalfont, UK.

using an ordered subset expectation maximization (OSEM) algorithm in all centers but Amsterdam (filtered backprojection). Attenuation correction was based on CT scan in Brescia, Genoa, and Marseille, and on transmission scan in Munich and Amsterdam. Scatter correction was performed using standard software as supplied by scanner manufacturers. Technical details of the scanners used in the different centers are reported in Table 2. Dicom files were exported and converted to Analyze format. Anonymous scans and clinical information are uploaded in a dedicated safe file transfer protocol (FTP) web site.

2.3. Imaging analysis

All preprocessing and statistical analysis steps were performed using SPM8 package (Wellcome Department of Cognitive Neurology, London, UK; Friston et al., 1994) implemented in Matlab 6.5 (MathWorks, Natick, Massachusetts, USA).

2.3.1. Customized 18F-FDG template editing and preprocessing of patients and controls brain FDG PET/CT

Because it was shown that the use of the tracer unmatched PET template to normalize brain scans may generate inconsistent results (Gispert et al., 2003) and because SPM default brain PET template is an $H_2{}^{15}O$ template, a customized brain FDG-PET template was built. The volumetric MRI scans of controls subjects acquired in Brescia were available in digital format. Therefore the study template was built from 27 brain PET and MRI scans of healthy subjects acquired there. This setting is the same as the default SPM setting (the template available for normalization is based on controls acquired in a single center which is "by definition" different from the center where the studied PET scans have been acquired). However, even if a gold standard on how a normalization template should be built has not been identified yet (Kas et al., 2007; Rosario et al., 2008), we cannot exclude that the inclusion of controls from other centers might have had a certain influence on the results of the following analyses.

Template editing was performed according to published procedure (Gispert et al., 2003; Meyer et al., 1999). Briefly, each FDG PET scan was first coregistered to the pertinent MRI scan (6 parameters, rigid body transformation) using the coregistration algorithm available in the SPM8 (Wellcome Department of Cognitive Neurology) package. Each magnetic resonance image was then spatially normalized to the SPM8 (Wellcome Department of Cognitive Neurology) T1-MRI template using an affine plus nonlinear transformation, and the resulting deformation field was applied to the coregistered FDG PET scan. The spatially normalized PET images were then averaged to obtain a mean PET image which was finally smoothed with an 8-mm isotropic Gaussian filter.

After template editing, all brain PET scans were subjected to affine and nonlinear spatial normalization into the Montreal Neurological Institute (MNI) space through the study-customized FDG template using SPM8 (Wellcome Department of Cognitive Neurology). The spatially normalized sets of images were then smoothed with a 10 mm isotropic Gaussian filter to blur individual variations in gyral anatomy and to increase the signal-to-noise ratio.

2.3.2. Definition of hypometabolic area in pAD patients

Prior to interregional correlation analysis, area of hypometabolism in pAD with respect to the whole group of 105 controls was assessed. This preliminary step aimed to identify regions of likely neuronal damage where an additional impairment of metabolic connectivity was evaluated by further correlation analysis.

Brain PET from pAD patients were compared on a voxel-by-voxel basis to those from the normal controls using "two-sample *t*-test" design of SPM8 (Wellcome Department of Cognitive Neurology). The significance of identified regions was established at a $p < 0.05$, corrected for multiple comparisons with the false discovery rate (FDR) option at both peak and cluster level. Only clusters containing more than 50 voxels were considered to be significant. Age and center were included in the analysis as confounding variables. As compared with controls, pAD showed relative hypometabolism in a large region including posterior parietal cortex, precuneus, and posterior cingulate cortex (PCC) in both hemispheres and lateral temporal lobe in the left hemisphere (Fig. 1). These clusters were finally saved and used as a single volumetric region of interest (VROI) in the subsequent connectivity analysis (hypometabolic area; HMA).

2.3.3. VROI analysis

All the analyzed VROIs were selected from the Pickatlas implemented in SPM (Maldjian et al., 2003). Among the metabolically preserved regions in the previous analysis, we selected 2 structures known to be involved in prodromal AD and 1 "control" region that has been reported to be substantially spared in the first stages of AD. Based on previous neuropathology and imaging studies, hippocampus (HC)

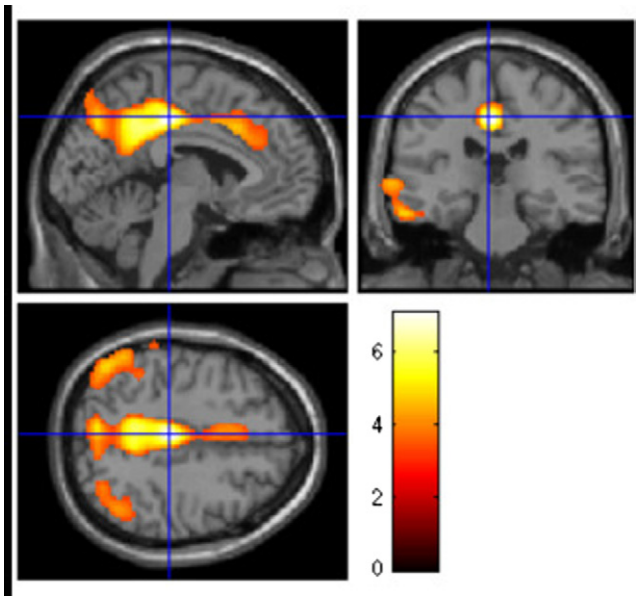

Fig. 1. Results of the comparison between prodromal Alzheimer's disease (pAD) patients and the whole group of 105 normal controls. The height threshold of significance was set at $p < 0.05$, corrected for multiple comparisons with the false discovery rate (FDR) option at both peak and cluster level. The figure displays regions of significant difference, color-graded in terms of Z values. pAD showed relative hypometabolism in a large region including posterior parietal cortex, precuneus, and posterior cingulate cortex in both hemispheres and lateral temporal lobe in the left hemisphere.

and dorsolateral-prefrontal cortex (DLFC) were chosen as prodromal AD-involved regions (Mosconi, 2005; Mosconi et al., 2004a, 2004b; Zelazo and Muller, 2002). According to the literature, DLFC was defined as the cortical area which includes Brodmann area (BA) 9 and 46. Sensorimotor area (SM), defined as BA 1, 2, 3, and 4, was selected as the "control" region. Left and right regions were evaluated independently. See Discussion for a more detailed explanation of these choices.

Mean FDG uptake within each of the 7 VROI (HMA, HC, DLFC, and SM bilaterally) was computed using SPM Mask subtool. Individual VROI FDG uptake values were then normalized to the individual mean uptake in the cerebellum (weighted FDG uptake).

2.3.4. Statistics: voxel-wise IRCA

Both in patient and control groups, extracted normalized mean regional VROI counts were used as covariates to find regions showing significant voxel-wise correlations across subjects using SPM8 (Wellcome Department of Cognitive Neurology) according to the procedure validated by Lee et al. (2008). Multiple regression analysis was chosen between the possible designs available in "Basic Models" function of SPM8 (Wellcome Department of Cognitive Neurology). This option allows the voxel-wise evaluation of the correlation between variables of interest and PET-assessed brain metabolism as well as nuisance effect (i.e., age and center of belonging) of each group independently. The gray matter threshold was set at 0.8. Normalization of global signal to 50 was performed with proportional scaling.

Age and center were included in the analysis as confounding variables. SPM T maps were displayed using an uncorrected $p < 0.001$ at peak level. This more liberal choice was adopted to avoid type II errors attributable to overconservative thresholds (Oishi et al., 2005). Effectively, given the exploratory nature of this analysis and considering the relatively low sensitivity of PET without repeated measures, higher thresholds could lead to false-negative results in PET studies. Clusters of correlations were regarded as significant if they survived at $p < 0.05$ threshold, FDR-corrected at cluster level. Only significant clusters containing at least 50 voxels were taken into consideration.

As apolipoprotein E (APOE) genotype was available only in 23 out of 36 patients, we could not include it as a nuisance variable in SPM analyses. Indeed, it has been demonstrated that APOEε4 carriers may show peculiar, and more extensive, regions of hypometabolism with respect to the general AD population (During et al., 2011; Mosconi et al., 2004a; Reiman et al., 2001). For this reason, the 23 patients whose APOE genotype was available were divided into APOE ε4+ ($n = 13$) and APOE ε4− ($n = 10$) subgroups and all IRCA analyses were repeated in the 2 subgroups (see Supplementary data). Correction of SPM coordinates to match the Talairach coordinates was achieved by the subroutine implemented by Matthew Brett (brainmap.org/index.html). BA were then identified at a range of 0 to 3 mm from the corrected Talairach coordinates of the SPM output isocenters, after importing the corrected coordinates, by Talairach client (www.talairach.org/index.html).

3. Results

3.1. Interregional correlation analysis of HMA

Resting metabolism in HMA correlated with several cortical areas in parietal, temporal, frontal, occipital, and limbic cortex in both hemispheres, and in left caudate nucleus in the 36 CTR group. These results were consistently replicated in the 69 CTR group (correlation with caudate nucleus in both hemispheres and with left thalamus). By contrast, the cluster of significant correlation substantially overlapped the HMA itself (autocorrelation) in pAD group. In fact, these clusters included bilateral posterior regions, such as superior parietal lobules, postcentral gyri, precuneus, and the angular gyrus in the right parietal lobe. The extension of this autocorrelation pattern in the parietal lobe was further reduced in the APOE ε4+ subgroup compared with both APOE ε4− subgroups and to the whole group of 36 pAD patients (Fig. 2, Table 3, and see Supplementary data).

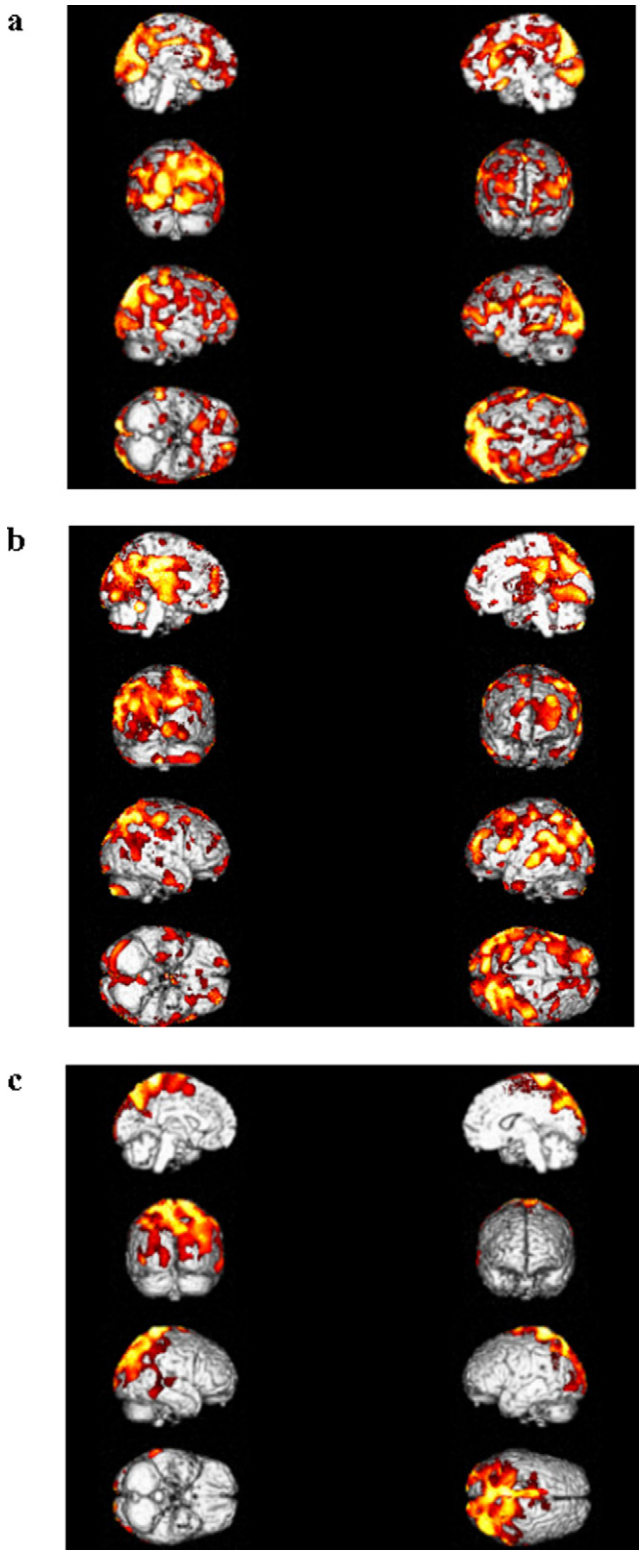

Fig. 2. Results of voxel-wise interregional correlation analysis (IRCA) of hypometabolic area (HMA) in the 36 normal control subjects (36CTR) (a) and 69 normal control subjects (69CTR) (b) groups and in prodromal Alzheimer's disease (pAD) group (c). The height threshold of significance was set at $p < 0.001$ uncorrected at peak level and at $p < 0.05$, corrected for multiple comparisons with the false discovery rate (FDR) option at cluster level. The figure displays regions of significant difference, color-graded in terms of Z values. Resting metabolism in hypometabolic area (HMA) correlated with several cortical areas in parietal, temporal, frontal, occipital, and limbic cortex in both hemispheres, and in left caudate nucleus both in 36CTR and 69CTR groups while the cluster of significant correlation substantially overlapped the HMA itself in pAD group. Talairach coordinates and further details are available in Table 3.

3.2. Interregional correlation analysis of HC metabolism

In the 36 CTR group, metabolism in both HC showed correlations with temporal, frontal, and occipital cortex and caudate nucleus, besides the expected autocorrelation. The results were consistently replicated in the 69 CTR group in which metabolism of both HC was also correlated with red nucleus in the left midbrain. In pAD, HC metabolism showed only autocorrelation and correlation with either the contralateral one (right HC) or amygdala (left HC) (Fig. 3, Table 4).

3.3. Interregional correlation analysis of DLFC metabolism

Metabolism in DLFC was extensively correlated with contralateral homologues and with little clusters in bilateral temporal, parietal cortex, and both caudate and putaminal nuclei in the 36 CTR group as well as in the 69 CTR group. Conversely, in the pAD group, left DLFC was substantially autocorrelated while right DLFC showed autocorrelation and a little cluster of correlation in the temporal and parietal cortex of the same hemisphere. When patients were divided into APOE $\varepsilon 4+$ and APOE $\varepsilon 4-$ subgroups, this little cluster was present only in APOE $\varepsilon 4-$ but not in APOE $\varepsilon 4+$ subgroup (Fig. 4, Table 5, and see Supplementary data).

3.4. Interregional correlation analysis of SM metabolism

Metabolic connectivity of SM in the 3 groups was substantially overlapping in both hemispheres. In fact, in all cases metabolism of SM was correlated with SM itself (autocorrelation) and with contralateral homologues (Fig. 5, Table 6).

4. Discussion

The main finding of this study is that interregional correlation of resting FDG uptake, assumed to reflect brain metabolic connectivity, is reduced in AD patients at the stage of aMCI with respect to age-matched healthy subjects and that this loss of metabolic connectivity affects both metabolically impaired and nonmetabolically impaired cortical and subcortical regions, thus disconnecting large-scale cognitive networks.

The applied SPM-based method of analysis had been validated in normal adults (aged between 19 and 55 years) (Lee et al., 2008) and has already been used to identify patterns of connectivity of posterior cingulate gyrus in the healthy condition (Vogt et al., 2006), of entorhinal cortex in

Table 3
Results of interregional correlation analysis of hypometabolic area in 36 normal control subjects (36 CTR), 69 normal control subjects (69 CTR), and prodromal Alzheimer's disease (pAD) patients

Analysis	Cluster level			Peak level			
	Cluster extent	Corrected p value	Cortical region	Maximum Z score	Talairach coordinates	Cortical region	BA
36 CTR	8000	0.001	R-parietal	6.59	70, −36, 32	Inferior parietal lobule	40
			R-parietal	6.42	26, −68, 28	Precuneus	7
			R-parietal	6.29	38, −22, 34	Post-central gyrus	2
			R-occipital	5.95	14, −82, 30	Cuneus	18
			L-parietal	5.91	−48, −44, 32	Supramarginal gyrus	40
			L-occipital	5.90	0, −74, −8,	Lingual gyrus	18
			L-limbic	5.75	−14, 28, 26	Cingulate gyrus	32
			R-limbic	5.00	24, −51, 7	Parahippocampal gyrus	30
	501	0.008	L-temporal	5.84	−39, −71, 31	Middle temporal gyrus	39
			R-frontal	5.40	18, 64, 38	Superior frontal gyrus	9
			R-frontal	5.36	4, 22, −24	Inferior frontal gyrus	47
	194	0.012	L-frontal	4.50	−14, 64, −18	Medial frontal gyrus	11
			R-caudate	3.90	14, 26, 12	Caudate body	
			L-caudate	3.88	−18, 24, 10	Caudate body	
69 CTR	4911	0.0001	R-parietal	6.26	22, −71, 61	Superior parietal lobule	7
			L-parietal	6.17	−30, −44, 48	Precuneus	7
			R-parietal	5.85	55, −17, 56	Post-central gyrus	3
			L-parietal	5.81	−49, −33, 31	Inferior parietal lobule	40
			L-parietal	5.79	−57, −9, 54	Post-central gyrus	3
			R-occipital	5.77	30, −99, −5,	Lingual gyrus	18
			L-occipital	4.86	−22, −71, 16	Precuneus	31
			L-limbic	4.00	0, −27, 35	Cingulate gyrus	31
			R-occipital	3.97	8, −98, 29	Cuneus	19
	1525	0.0001	L-temporal	5.78	−38, −70, 31	Middle temporal gyrus	39
			L-frontal	5.60	−65, 13, 25	Inferior frontal gyrus	9
			L-frontal	5.44	−46, 20, 14	Inferior frontal gyrus	45
			L-frontal	5.11	−44, 1, 29	Precentral gyrus	6
			L-caudate	5.05	−18, 24, 11	Caudate body	
	683	0.001	R-limbic	5.03	16, −66, 7	Posterior cingulate	30
			R-limbic	4.99	24, −52, 6	Parahippocampal gyrus	30
	187	0.011	L-thalamus	4.86	−4, −9, 19	Thalamus	
pAD	8240	0.001	R-parietal	4.40	34, −54, 56	Superior parietal lobule	7
			R-parietal	4.27	40, −36, 64	Postcentral gyrus	2
			L-parietal	4.22	−34, −79, 46	Precuneus	19
			L-parietal	4.16	−30, −73, 50	Superior parietal lobule	7
			L-parietal	3.96	−24, −37, 70	Postcentral gyrus	2
			R-parietal	3.85	30, −71, 50	Precuneus	7
			L-parietal	3.81	−42, −52, 47	Inferior parietal lobule	40
			R-temporal	3.79	44, −74, 30	Angular gyrus	39

Uncorrected $p < 0.001$ at peak level and $p < 0.05$, false discovery rate corrected at cluster level, were accepted as statistically significant. In the "cluster level" section on the left, for each cluster found to be statistically significant, the number of voxels, the corrected p value and the cortical region where the cluster is found, are reported. In the "peak level" section on the right, for each significant cluster, the peak coordinates and Z score, the corresponding cortical region and Brodmann area (BA) are reported. L, left; R, right.

patients with AD at the stage of dementia (Mosconi et al., 2004b) as well as changes in connectivity during the development of profound deaf subjects (Kang et al., 2003). Accordingly, the present results in two independent control groups extend to a healthy elderly population the normative data published in young adults. Regional brain glucose metabolic distribution mainly reflects local metabolism at the synaptic level, as the greater part of glucose utilization happens there (Gruetter et al., 2003; Hyder et al., 2006; Magistretti and Pellerin, 1999; Price and Morris, 1999). In previous studies, interregional correlations of metabolic glucose rates were discussed in terms of "traffic (metabolic-functional connectivity) in the anatomical 'roads' present in the brain" which, by contrast, can be investigated by other neuroimaging methods such as diffusion tensor imaging (Lee et al., 2008). The prodromal stage of AD is particularly suited for a resting metabolic connectivity analysis for pathophysiological reasons. First, degeneration of neuronal synapses and processes is thought to precede neuronal death for a substantial period (Lacor et al., 2007); second, several lines of evidence suggest that in the preclinical stage of AD, β-amyloid deposition is mainly present in DMN regions (Drzezga et al., 2011); third, the high sensitivity of FDG-PET is ideal in highlighting the initial and subtle alteration of brain function in the very early stage of AD. In the present study, the analysis of both metabolically impaired and not significantly impaired cortical and subcortical regions has contributed to further disclose the potential of

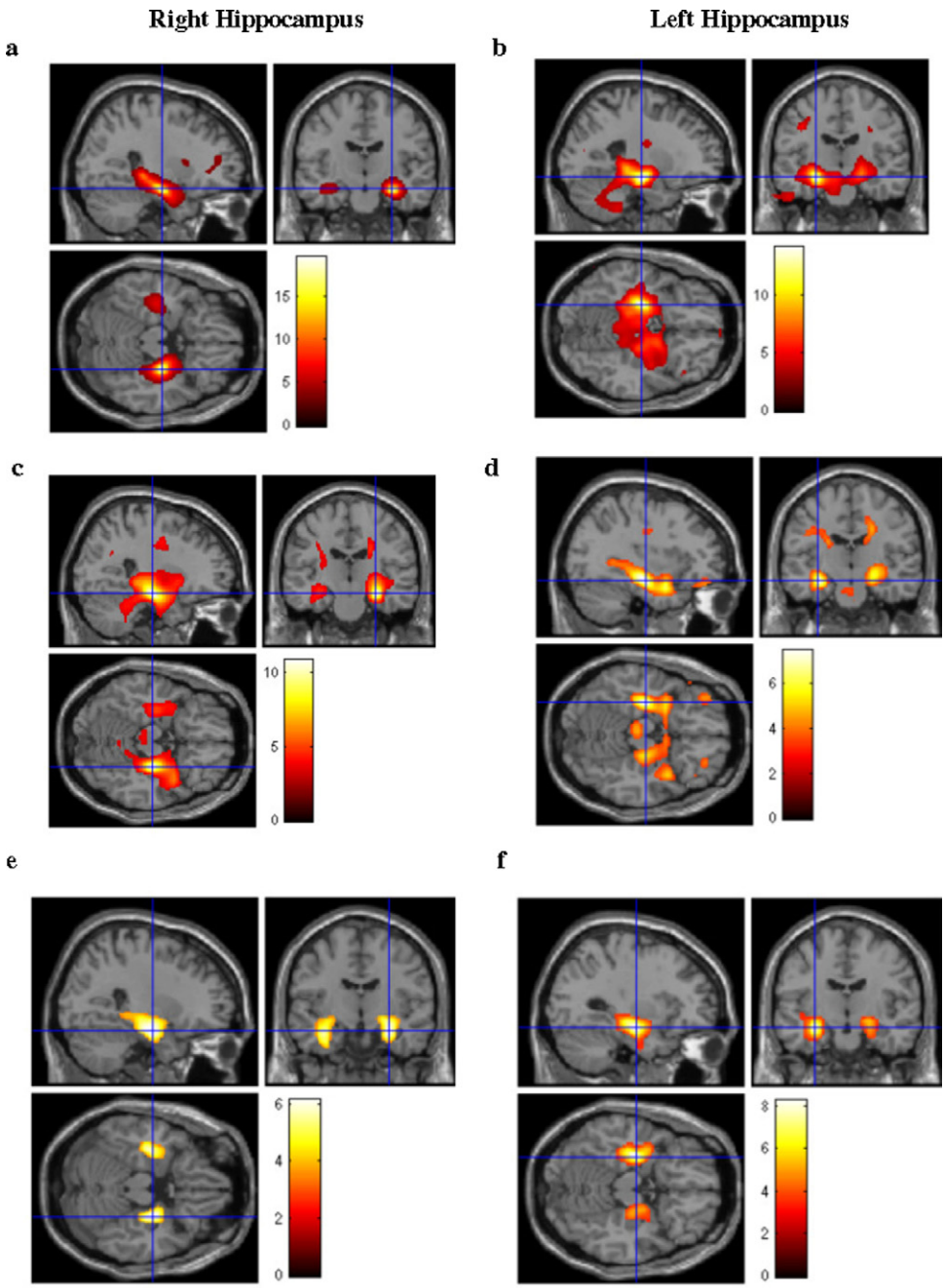

Fig. 3. Results of voxel-wise interregional correlation analysis (IRCA) of right and left hippocampi (HC) in the 36 normal control subjects (36CTR) (a, b) and 69 normal control subjects (69CTR) (c, d) groups and in prodromal Alzheimer's disease (pAD) group (e, f). In both 36CTR and 69CTR groups, metabolism HC showed, besides the expected autocorrelation, correlations with temporal, frontal, and occipital cortex and caudate nucleus bilaterally while in pAD, HC metabolism showed only autocorrelation and correlation with either the contralateral one (right HC) or amygdala (left HC). Talairach coordinates and further details are available in Table 4.

brain FDG imaging in the evaluation of both neuronal and synaptic activity.

In fact, as expected, pAD patients showed relative hypometabolism in a region including posterior parietal cortex, precuneus and PCC in both hemispheres as compared with controls. In both control groups these regions showed to be metabolically correlated with several cortical areas in parietal, temporal, frontal, limbic, and occipital cortex in both hemispheres while they were substantially just autocorrelated in the patient group. From the methodological point of view, it might be argued that in patients the mere presence of hypometabolism in posterior associative and limbic cortex could have been responsible for a decreased correlation with the other "metabolically spared" regions.

Table 4
Results of interregional correlation analysis of left (A) and right (B) hippocampus area in 36 normal control subjects (36 CTR), 69 normal control subjects (69 CTR), and prodromal Alzheimer's disease (pAD) patients

Analysis	Cluster extent	Corrected p value	Cortical region	Maximum Z score	Talairach coordinates	Cortical region	BA
A.	Cluster level			Peak level			
36 CTR	1354	0.001	L-limbic	14.25	−24, −16, −11	Hippocampus	
			R-limbic	8.84	22, −20, −6	Parahippocampal gyrus	28
			L-temporal	8.22	−61, −61, −15	Inferior temporal gyrus	20
			L-temporal	5.61	−55, −69, −17	Fusiform gyrus	19
			R-temporal	5.39	48, 10, −34	Middle temporal gyrus	21
	347	0.003	R-occipital	5.12	18, −75, 18	Cuneus	18
			R-occipital	3.92	40, −79, −16	Fusiform gyrus	19
			R-limbic	3.85	18, 6, 42	Cingulate gyrus	32
	267	0.03	R-frontal	4.96	51, 25, −8	Inferior frontal gyrus	47
			R-frontal	4.78	−40, −14, 36	Precentral gyrus	6
			R-frontal	4.40	6, 63, −15	Medial frontal gyrus	4
			L-frontal	3.96	−36, −1, 28	Precentral gyrus	6
			R-caudate	3.78	20, −7, 22	Caudate body	
	69	0.05	R-limbic	4.67	−18, 24, 10	Cingulate gyrus	32
69 CTR	2415	0.0001	L-limbic	7.47	−32, −16, −13	Hippocampus	
			L-limbic	6.44	−28, 3, −20	Uncus	28
			R-limbic	4.35	24, −20, −7	Parahippocampal gyrus	28
			R-limbic	4.00	22, −9, −33	Uncus	36
			R-temporal	3.78	40, 5, −12	Superior temporal gyrus	38
			L-midbrain	3.50	−2, −23, −14	Red nucleus	
	533	0.003	R-occipital	5.40	8, −96, −7	Lingual gyrus	18
	1316	0.0001	R-frontal	4.91	30, 40, −19	Middle frontal gyrus	11
			R-frontal	4.74	30, 30, −25	Inferior frontal gyrus	11
			L-frontal	4.72	−65, 16, 5	Inferior frontal gyrus	45
			L-frontal	4.45	−36, 42, −17	Superior frontal gyrus	11
			L-frontal	4.36	−40, −10, 32	Precentral gyrus	6
			L-frontal	3.90	−53, 28, −13	Inferior frontal gyrus	47
			L-caudate	3.86	−22, −14, 23	Caudate body	
			R-caudate	3.82	4, 2, 2	Caudate head	
pAD	1535	0.0001	L-limbic	8.26	−30, −12, −13	Hippocampus	
			L-limbic	3.92	−34, −9, −28	Uncus	20
	719	0.002	R-amygdala	5.40	20, −10, −8	Amygdala	
B.	Cluster level			Peak level			
36 CTR	4424	0.0001	R-limbic	19.60	28, −14, −14	Hippocampus	
			L-limbic	10.34	−36, −20, −12	Hippocampus	
			R-temporal	8.22	51, 9, −6	Superior temporal gyrus	22
	167	0.03	R-occipital	6.27	16, −65, 20	Precuneus	31
			R-limbic	5.29	10, −42, 13	Posterior cingulate	29
			L-limbic	5.05	−10, −50, 17	Posterior cingulate	30
	98	0.012	R-frontal	4.90	28, 43, 11	Middle frontal gyrus	10
			R-frontal	4.81	28, 35, 0	Inferior frontal gyrus	47
			R-frontal	4.79	8, 14, 42	Medial frontal gyrus	6
			L-frontal	4.78	−24, 58, 38	Superior frontal gyrus	9
			R-caudate	4.40	18, 18, 5	Caudate body	
69 CTR	7345	0.0001	R-limbic	10.83	28, −18, −13	Hippocampus	
			R-temporal	5.83	42, 3, −14	Superior temporal gyrus	38
			L-limbic	5.35	−34, −1, −22	Amygdala	
			L-limbic	5.00	−32, −12, −15	Hippocampus	
			L-temporal	4.90	−34, 5, −10	Superior temporal gyrus	38
			L-midbrain	3.02	−2, −24, −14	Red nucleus	
	899	0.0001	R-parietal	5.56	26, −57, 29	Precuneus	7
			L-parietal	5.03	−20, −32, 59	Postcentral gyrus	3
	561	0.002	R-frontal	5.36	20, 25, 28	Medial frontal gyrus	9
			R-frontal	3.73	53, 36, 26	Middle frontal gyrus	46
			L-frontal	3.71	−20, −3, 61	Middle frontal gyrus	6
			L-frontal	3.66	−28, 19, 30	Middle frontal gyrus	9
			L-frontal	3.54	−44, 57, 19	Superior frontal gyrus	10
			R-caudate	3.33	20, 16, 14	Caudate body	
			L-caudate	3.29	−10, 23, −5	Caudate head	
pAD	1334	0.0001	R-limbic	6.15	28, −11, −16	Hippocampus	
	1132	0.001	L-limbic	5.72	−36, −12, −16	Hippocampus	

Uncorrected $p < 0.001$ at peak level and $p < 0.05$, false discovery rate corrected at cluster level, were accepted as statistically significant. In the "cluster level" section on the left, for each cluster found to be statistically significant, the number of voxels, the corrected p value and the cortical region where the cluster is found are reported. In the "peak level" section on the right, for each significant cluster, the peak coordinates and Z score, the corresponding cortical region and Brodmann area (BA) are reported. L, left; R, right.

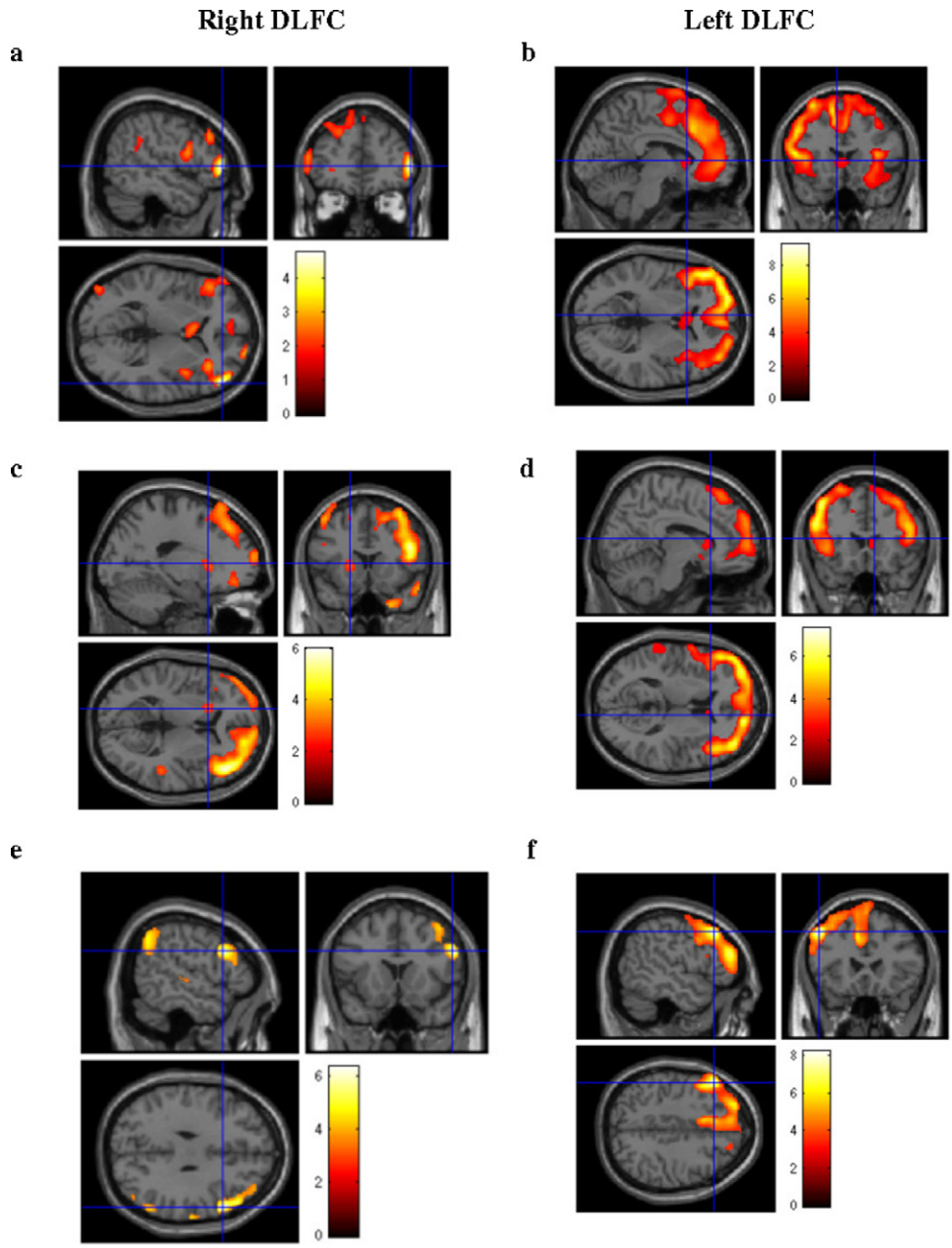

Fig. 4. Results of voxel-wise interregional correlation analysis (IRCA) of right and left dorsolateral-prefrontal cortex (DLFC) in the 36 normal control subjects (36CTR) (a, b) and 69 normal control subjects (69CTR) (c, d) groups and in prodromal Alzheimer's disease (pAD) group (e, f). Metabolism in DLFC was correlated with contralateral homologues and with little clusters in bilateral temporal, parietal cortex, and both caudate and putaminal nuclei in control groups while in the pAD group, left DLFC was substantially autocorrelated while right DLFC showed autocorrelation and a little cluster of correlation in the temporal and parietal cortex of the same hemisphere. Talairach coordinates and further details are available in Table 5.

This argument cannot be definitely ruled out, but the anatomo-physiological coherence of the findings and the reduced functional connectivity highlighted also in brain regions with preserved metabolism strongly suggest a pathophysiological interpretation. Moreover, the absence of significant modifications of metabolic connectivity in the SM in pAD compared with controls further testifies the specificity of the present findings.

PCC hypometabolism is among the most common findings in FDG-PET studies of early AD (de Leon et al., 1983; Minoshima et al., 1997; Morbelli et al., 2010). More recently, functional deactivation profiles in the PCC were shown to differ between patients with AD and healthy controls (Lustig et al., 2003). For these reasons, the leading hypothesis is that decreased PCC activity in prodromal AD reflects decreased connectivity especially with entorhinal cortex and hippocampus, which are among the first regions targeted by AD pathology (Me-

Table 5
Results of interregional correlation analysis of left (A) and right (B) DLFC area in 36 normal control subjects (36 CTR), 69 normal control subjects (69 CTR), and prodromal Alzheimer's disease patients (pAD)

Analysis	Cluster extent	Corrected *p* value	Cortical region	Maximum *Z* score	Talairach coordinates	Cortical region	BA
A.	Cluster level			Peak level			
36 CTR	26,510	0.0001	L-frontal	9.47	51, 37, 9	Inferior frontal gyrus	46
			L-frontal	9.17	−10, 25, 39	Medial frontal gyrus	8
			L-frontal	8.75	−10, −13, 58	Medial frontal gyrus	6
			L-frontal	8.69	−53, −3, 61	Precentral gyrus	6
			R-frontal	8.39	28, 34, 54	Superior frontal gyrus	8
			R-frontal	8.34	36, 14, 40	Precentral gyrus	9
			R-frontal	8.34	30, −2, 68	Superior frontal gyrus	6
			R-frontal	8.10	51, 11, 23	Inferior frontal gyrus	44
			R-caudate	7.92	10, 12, 10	Caudate body	
			L-caudate	7.75	−2, 18, 3	Caudate head	
			L-parietal	7.39	−63, −38, 50	Inferior parietal lobule	40
			L-parietal	7.17	−65, −51, 34	Supramarginal gyrus	40
			L-putamen	6.92	−18, 12, 10	Lentiform nucleus	
69 CTR	22,950	0.0001	L-frontal	7.36	53, 27, 26	Middle frontal gyrus	46
			L-frontal	6.60	−40, 44, 25	Middle frontal gyrus	10
			R-frontal	6.38	50, 4, 48	Middle frontal gyrus	6
			R-frontal	6.29	40, 5, −18	Superior frontal gyrus	6
			R-caudate	6.11	8, 18, 5	Caudate body	40
			R-putamen	5.90	14, 8, −4	Lentiform nucleus	7
			L-caudate	5.69	−16, 16, 8	Caudate body	40
			L-parietal	5.20	−55, −53, 28	Supramarginal gyrus	21
			L-parietal	5.06	−16, −68, 40	Precuneus	22
			R-parietal	5.01	53, −37, 44	Inferior parietal lobule	31
	517	0.001	L-temporal	5.10	−55, 8, −26	Middle temporal gyrus	
			R-temporal	4.90	69, −25, 1	Superior temporal gyrus	
			R-temporal	3.98	0, −55, 23	Posterior cingulate	
pAD	10,140	0.0001	L-frontal	8.24	−46, 44, 20	Middle frontal gyrus	46
			L-frontal	7.43	−38, 46, 27	Middle frontal gyrus	9
			L-frontal	7.04	−49, 25, 39	Middle frontal gyrus	8
			L-frontal	6.96	−40, 53, 7	Middle frontal gyrus	10
			L-frontal	6.88	−8, 12, 53	Superior frontal gyrus	6
			L-frontal	6.84	−8, 23, 34	Cingulate gyrus	32
			R-frontal	6.79	2, 32, 59	Superior frontal gyrus	6
			R-frontal	6.21	16, 39, 50	Superior frontal gyrus	8
B.	Cluster level			Peak level			
36 CTR	3833	0.0001	R-frontal	5.19	44, 13, 27	Middle frontal gyrus	9
			R-frontal	5.06	59, 26, 21	Inferior frontal gyrus	45
			R-frontal	4.98	34, 8, 53	Middle frontal gyrus	6
			R-frontal	4.85	22, 68, 6	Superior frontal gyrus	10
			L-frontal	4.78	−34, 27, 43	Middle frontal gyrus	8
			L-frontal	4.71	−22, 5, 61	Superior frontal gyrus	6
			L-caudate	4.60	−6, 18, 6	Caudate Bbody	40
	982	0.001	R-parietal	4.82	44, −39, 30	Supramarginal gyrus	40
			R-parietal	4.74	50, −47, 61	Inferior Parietal Llobe	40
			L-parietal	4.71	−38, −58, 40	Inferior Parietal Llobe	38
			R-temporal	4.40	30, 14, −38	Superior Temporal gyrus	18
			L-occipital	3.98	25, −14, −104	Cuneus	
69 CTR	13,780	0.0001	R-frontal	6.00	48, 26, 13	Inferior frontal gyrus	46
			R-frontal	5.84	48, 40, 16	Middle frontal gyrus	46
			L-frontal	5.79	−48, 43, −4	Inferior frontal gyrus	10
			L-frontal	5.20	−18, 39, 40	Superior frontal gyrus	8
			R-caudate	5.05	8, 21, 3	Caudate head	2
			R-putamen	3.83	18, 8, 0	Lentiform nucleus	21
			L-putamen	3.73	−18, 16, 3	Lentiform nucleus	38
	3479	0.0001	R-parietal	5.20	69, −22, 27	Postcentral gyrus	36
			R-temporal	5.05	59, 1, −12	Middle temporal gyrus	
			R-temporal	4.41	28, 16, −31	Superior temporal gyrus	
			R-limbic	3.73	36, −20, −21	Parahippocampal gyrus	

(continued on next page)

Table 5
(continued)

Analysis	Cluster extent	Corrected p value	Cortical region	Maximum Z score	Talairach coordinates	Cortical region	BA
pAD	1882	0.0001	R-frontal	6.33	55, 17, 27	Middle frontal gyrus	9
			R-frontal	5.53	40, 53, 7	Middle frontal gyrus	10
			R-frontal	5.50	42, 22, 47	Middle frontal gyrus	8
	1306	0.002	R-parietal	5.13	51, −58, 45	Inferior parietal lobule	40
			R-parietal	4.93	34, −71, 48	Superior parietal lobule	7
	1177	0.002	R-temporal	5.07	65, −17, 1	Superior temporal gyrus	22

Uncorrected $p < 0.001$ at peak level and $p < 0.05$, false discovery rate corrected at cluster level, were accepted as statistically significant. In the "cluster level" section on the left, for each cluster found to be statistically significant, the number of voxels, the corrected p value and the cortical region where the cluster is found are reported. In the "peak level" section on the right, for each significant cluster, the peak coordinates and Z score, the corresponding cortical region and Brodmann area (BA) are reported. DLFC, dorsolateral prefrontal cortex; L, left; R, right.

guro et al., 1999). This evidence is supported by hypometabolic changes in PCC after rhinal cortex ablation (Meguro et al., 1999). In keeping with this hypothesis, the present study highlights the correlation between hypometabolic PCC-posterior parietal cortex and entorhinal cortex (namely, parahippocampal gyrus) in two independent groups of controls. However, we failed to find hippocampal hypometabolism in the comparison between patients and controls which is common when using voxel-based analysis of FDG PET (Mosconi, 2005). In fact, while several observations suggest that early hippocampal structural brain damage of AD is coupled with hypofunction and specifically reduced brain glucose metabolism, hippocampal hypometabolism is often not reported probably also in relation to both PET resolution and, particularly, the SPM analysis method (see Mosconi, 2005, for deep discussion of this issue). Accordingly, due both to its pathophysiological importance and to the above technical challenges, hippocampal metabolic connectivity was specifically and separately analyzed in this study. In both the groups of controls, the hippocampi showed correlations with themselves, contralateral homologues, and with temporal, frontal, occipital cortex, and caudate nuclei; conversely, only autocorrelation plus correlation with contralateral homologues was present in the pAD group. In a previous FDG PET study focusing on entorhinal cortex connectivity at the stage of dementia (Mosconi et al., 2004b), it was shown that in healthy controls entorhinal cortex shares reciprocal interconnections with the hippocampus and the parahippocampal cortex, and receives inputs from the orbital and dorsolateral frontal cortex, the parietotemporal and occipital associative areas, and the cingulate cortex. By contrast, as compared with the wide brain system outlined in controls, in AD patients there was a loss of significant entorhinal cortex functional interactions. The present study further supports already at the aMCI stage of AD, the concept of metabolic disconnection of medial temporal lobe reported in AD-dementia, as the "whole brain" nature of SPM voxel-based analysis allows full topographic exploration of metabolic connections of a defined brain region (Hyman et al., 1984).

Resting fMRI studies (Greicius et al., 2004) demonstrated that hippocampus plays a prominent role in the DMN and that, in this context, its functional activity and connectivity is compromised in AD as compared with healthy elderly controls.

In the present study, both hippocampi showed correlation with the cuneus, precuneus, and posterior cingulate in both control groups, but not in pAD patients. These findings are consistent with previous fMRI studies of "'resting state'" functional connectivity suggesting that even when not engaged in a specific task, the hippocampus is functionally connected to the DMN, in particular to posteromedial regions extending from posterior cingulate to precuneus (Greicius et al., 2004; Kahn et al., 2008; Vincent et al., 2006). The lack of the above-mentioned metabolic correlation in the pAD group is thus in keeping with the reported perturbation of DMN in AD (Greicius et al., 2004) thought to lead to abnormalities in large-scale memory networks (Dickerson and Sperling, 2009). Of note, the extension of the cluster of autocorrelation of both hippocampi is limited in pAD with respect to both control groups. This finding may reflect reduced within-lobe connectivity in prodromal AD and is in agreement with a recent study on functional connectivity of brain FDG PET investigated by means of sparse inverse covariance estimation (Huang et al., 2010).

Among the remaining associative cortical regions not significantly impaired in the pAD group, we chose to analyze metabolic connectivity of the DLFC because of its dense connection with hippocampus in the memory-related networks (Zelazo and Muller, 2002) and to its emerging role in the discrimination between MCI rapidly converting to dementia of Alzheimer's type and stable MCI (Mosconi et al., 2004b, 2004c). Moreover, the connectivity of most posterior associative cortex had been already evaluated as a part of the hypometabolic area.

DLFC showed correlation with contralateral homologues, bilateral temporal, parietal cortex, and basal ganglia in both control groups while it was only autocorrelating or, in the right cerebrum, just correlating with ipsilateral temporal and parietal cortex in the pAD group. Thus, in pAD patients metabolic connectivity was lack-

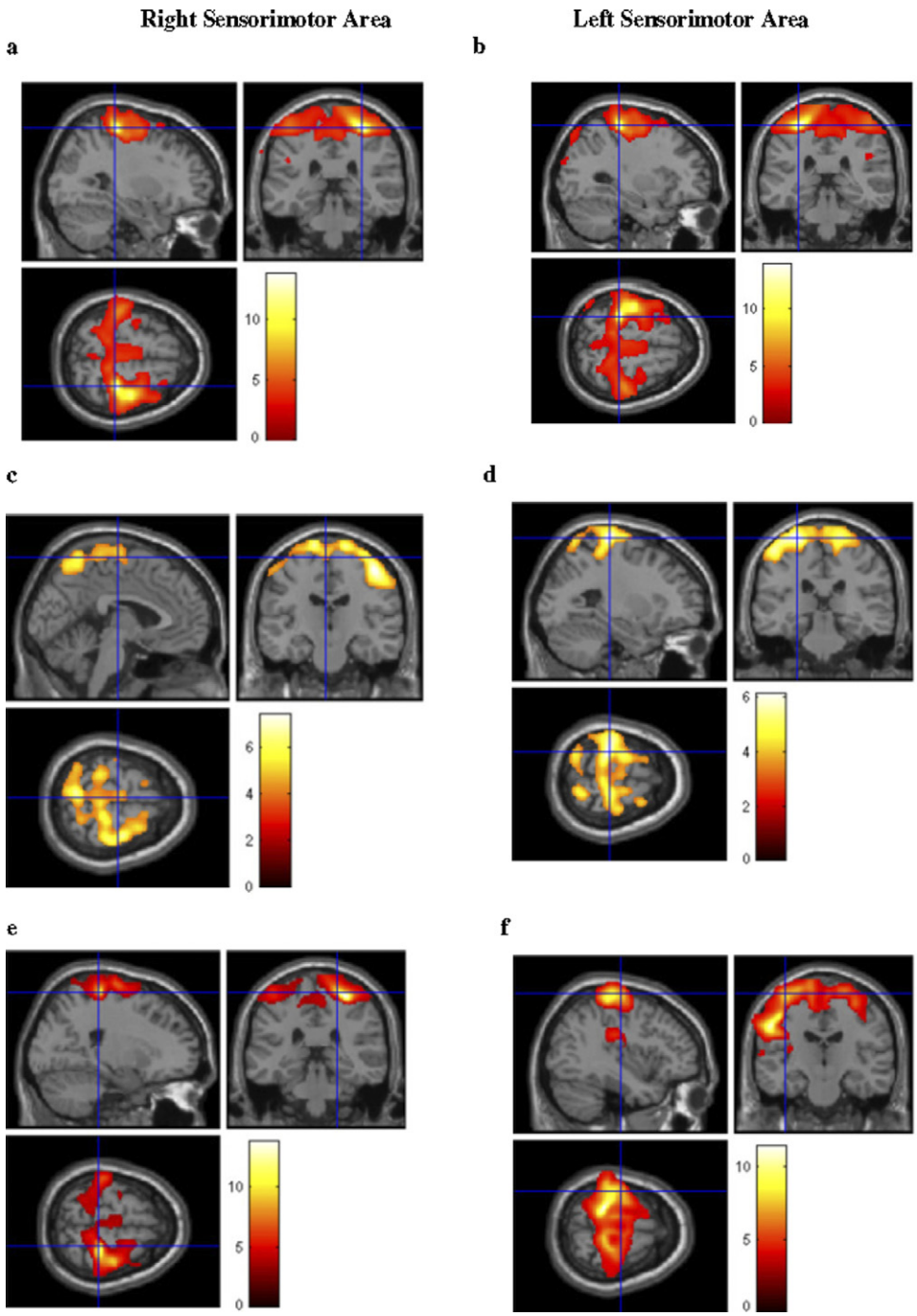

Fig. 5. Results of voxel-wise interregional correlation analysis (IRCA) of right and left sensorimotor (SM) area in the 36 normal control subjects (36CTR) (a, b) and 69 normal control subjects (69CTR) (c, d) groups and in prodromal Alzheimer's disease (pAD) group (e, f). Metabolic connectivity of SM of both hemispheres was very similar among the 3 groups. In all groups metabolism of SM was correlated with SM itself (autocorrelation) and with the contralateral homologues. Talairach coordinates and further details are available in Table 6.

ing between frontal cortex and both PCC-posterior parietal regions and hippocampus. In previous VROI-based FDG PET studies, a loss of frontal-parietal regional interactions was reported in the early stages of AD (Azari et al., 1992; Horwitz et al., 1987). Moreover, coherent with a large presence of frontal lobe correlations in almost all the present resting metabolic connectivity analysis, both control groups showed interregional correlations involving caudate nuclei of both hemispheres. These findings, likely to reflect the effect of fronto-

Table 6
Results of interregional correlation analysis of left (A) and right (B) sensorimotor area in 36 normal control subjects (36 CTR), 69 normal control subjects (69 CTR) and prodromal Alzheimer's disease patients (pAD)

Analysis	Cluster extent	Corrected *p* value	Cortical region	Maximum *Z* score	Talairach coordinates	Cortical region	BA
A.	Cluster level			Peak level			
36 CTR	22,050	0.001	L-frontal	7.25	−30, −28, 59	Precentral gyrus	4
			L-parietal	6.77	−44, −19, 53	Postcentral gyrus	3
			L-frontal	6.74	−18, −10, 71	Superior frontal gyrus	6
			R-parietal	5.71	46, −24, 64	Postcentral gyrus	3
			L-frontal	5.22	−6, −12, 69	Medial frontal gyrus	6
			R-frontal	5.07	26, −4, 67	Superior frontal gyrus	6
			R-parietal	4.69	32, −34, 62	Postcentral gyrus	2
			L-parietal	4.62	−44, −63, 57	Superior parietal lobule	7
			R-parietal	4.46	24, −42, 63	Postcentral gyrus	5
			R-frontal	4.36	10, −16, 71	Superior frontal gyrus	6
			L-frontal	4.02	−4, 29, 59	Middle frontal gyrus	6
			R-parietal	4.02	67, −21, 40	Postcentral gyrus	1
			L-parietal	3.97	−61, −42, 48	Inferior parietal lobule	40
			R-frontal	3.91	16, −29, 51	Subgyral	4
			L-parietal	3.9	−61, −53, 38	Supramarginal gyrus	40
			L-parietal	3.89	−32, −75, 52	Superior parietal lobule	7
			L-frontal	3.87	−26, 19, 60	Middle frontal gyrus	6
			R-frontal	3.79	10, 6, 72	Superior frontal gyrus	6
			L-parietal	3.62	−57, −56, 43	Inferior parietal lobule	40
			L-temporal	3.59	−51, −73, 13	Middle temporal gyrus	39
69 CTR	7961	0.0001	L-parietal	7.12	−18, −32, 68	Postcentral gyrus	3
			L-frontal	7	−53, −14, 34	Precentral gyrus	4
			R-frontal	6.32	8, −29, 71	Paracentral lobule	6
			L-parietal	5.91	−51, −24, 60	Postcentral gyrus	1
			R-frontal	5.78	18, −28, 64	Precentral gyrus	4
			L-parietal	5.73	−48, −26, 62	Postcentral gyrus	3
			L-frontal	5.67	−28, −10, 67	Precentral gyrus	6
			R-frontal	5.51	32, −18, 58	Precentral gyrus	4
			R-frontal	5.18	6, −10, 65	Medial frontal gyrus	6
			L-temporal	5.12	−53, −30, 13	Superior temporal gyrus	42
			L-frontal	4.98	−14, 11, 62	Superior frontal gyrus	6
			R-frontal	4.75	30, −28, 59	Precentral gyrus	4
			R-frontal	4.75	38, −15, 56	Precentral gyrus	4
			R-parietal	4.73	44, −19, 53	Postcentral gyrus	3
			R-frontal	4.60	42, −17, 45	Postcentral gyrus	4
			R-frontal	4.58	18, −10, 71	Superior frontal gyrus	6
			L-parietal	4.54	−46, −17, 47	Postcentral gyrus	3
			R-parietal	4.51	12, −34, 61	Postcentral gyrus	3
			R-frontal	4.47	44, −16, 28	Precentral gyrus	6
			L-frontal	4.30	−26, −4, 67	Superior frontal gyrus	6
			L-parietal	4.28	−32, −34, 62	Postcentral gyrus	2
			L-frontal	4.12	−16, −34, 59	Postcentral gyrus	4
			L-parietal	4.00	−24, −42, 63	Postcentral gyrus	5
			L-frontal	3.9	−10, −16, 71	Superior frontal gyrus	6
			R-frontal	3.91	42, 9, 59	Middle frontal gyrus	6
			L-parietal	3.64	−67, −21, 40	Postcentral gyrus	1
			R-frontal	3.20	26, 19, 60	Superior frontal gyrus	6
			L-frontal	3.18	−10, 6, 72	Superior frontal gyrus	6
			L-frontal	3.10	−8, 11, 66	Superior frontal gyrus	6
			L-parietal	3.09	−46, −26, 29	Postcentral gyrus	2
pAD	23,584	0.0001	L-frontal	8.27	−30, −28, 59	Precentral gyrus	4
			L-parietal	5.35	−44, −19, 53	Postcentral gyrus	3
			R-parietal	5.12	46, −24, 64	Postcentral gyrus	3
			L-frontal	4.73	−6, −12, 69	Medial frontal gyrus	6
			R-frontal	4.69	26, −4, 67	Superior frontal gyrus	6
			R-parietal	4.58	32, −34, 62	Postcentral gyrus	2
			L-parietal	4.54	−44, −63, 57	Superior parietal lobule	7
			R-parietal	4.51	24, −42, 63	Postcentral gyrus	5
			R-frontal	4.18	10, −16, 71	Superior frontal gyrus	6
			L-frontal	4.00	−42, 9, 59	Middle frontal gyrus	6
			R-parietal	3.9	67, −21, 40	Postcentral gyrus	1

(continued on next page)

Table 6
(Continued)

Analysis	Cluster extent	Corrected p value	Cortical region	Maximum Z score	Talairach coordinates	Cortical region	BA
			L-parietal	3.91	−61, −42, 48	Inferior parietal lobule	40
			R-frontal	3.72	16, −29, 51	Subgyral	4
			L-parietal	3.20	−32, −75, 52	Superior parietal lobule	7
			L-frontal	3.18	−26, 19, 60	Middle frontal gyrus	6
			R-frontal	3.10	10, 6, 72	Superior frontal gyrus	6
			L-temporal	3.09	−51, −73, 13	Middle temporal gyrus	39
B.	Cluster level			Peak level			
36 CTR	17,852	0.0001	R-frontal	7.25	30, −28, 59	Precentral gyrus	4
			R-parietal	6.77	44, −19, 53	Postcentral gyrus	3
			R-frontal	6.74	42, −17, 45	Postcentral gyrus	4
			R-frontal	5.71	18, −10, 71	Superior frontal gyrus	6
			R-frontal	5.07	6, −12, 69	Medial frontal gyrus	6
			L-parietal	4.69	−46, −17, 47	Postcentral gyrus	3
			R-parietal	4.62	12, −34, 61	Postcentral gyrus	3
			R-frontal	4.46	44, −16, 28	Precentral gyrus	6
			L-frontal	4.36	−26, −4, 67	Superior frontal gyrus	6
			L-parietal	4.02	−32, −34, 62	Postcentral gyrus	2
			L-frontal	3.97	−10, −16, 71	Superior frontal gyrus	6
			R-frontal	3.91	42, 9, 59	Middle frontal gyrus	6
			L-parietal	3.9	−67, −21, 40	Postcentral gyrus	1
			L-frontal	3.87	−16, −29, 51	Precentral gyrus	4
			R-frontal	3.79	26, 19, 60	Superior frontal gyrus	6
			L-frontal	3.62	−10, 6, 72	Superior frontal gyrus	6
			L-frontal	3.59	−8, 11, 66	Superior frontal gyrus	6
			L-parietal	3.59	−46, −26, 29	Postcentral gyrus	2
69 CTR	7345	0.0001	R-frontal	7.06	30, −28, 59	Precentral gyrus	4
			R-frontal	6.32	42, −18, 46	Postcentral gyrus	4
			R-frontal	5.91	18, −10, 71	Superior frontal gyrus	6
			L-parietal	5.78	−46, −24, 64	Postcentral gyrus	3
			R-frontal	5.73	6, −12, 68	Medial frontal gyrus	6
			L-frontal	5.67	−25, −4, 67	Superior frontal gyrus	6
			L-parietal	4.54	−32, −34, 62	Postcentral gyrus	2
			L-parietal	4.47	−24, −42, 63	Postcentral gyrus	5
			L-frontal	4.28	−10, −16, 71	Superior frontal gyrus	6
			L-parietal	4.13	−67, −21, 39	Postcentral gyrus	1
			L-frontal	3.95	−16, −29, 51	Precentral gyrus	4
			R-frontal	3.91	26, 19, 60	Superior frontal gyrus	6
			L-frontal	3.64	−10, 7, 72	Superior frontal gyrus	6
			L-frontal	3.08	−8, 11, 66	Superior frontal gyrus	6
			L-parietal	3.06	−46, −26, 29	Postcentral gyrus	2
			R-frontal	3.00	42, 9, 59	Middle frontal gyrus	6
pAD	11,470	0.0001	R-parietal	6.32	44, −19, 53	Postcentral gyrus	3
			R-frontal	5.91	42, −17, 45	Postcentral gyrus	4
			R-frontal	5.78	19, −10, 71	Superior frontal gyrus	6
			L-parietal	5.73	−46, −24, 64	Postcentral gyrus	3
			R-frontal	5.67	6, −12, 69	Medial frontal gyrus	6
			L-parietal	5.18	−32, −34, 62	Postcentral gyrus	2
			L-frontal	5.12	−11, −16, 71	Superior frontal gyrus	6
			L-parietal	4.54	−67, −22, 40	Postcentral gyrus	1
			L-frontal	4.47	−16, −29, 51	Precentral gyrus	4
			R-frontal	4.28	27, 19, 60	Superior frontal gyrus	6
			L-frontal	4.02	−10, 6, 72	Superior frontal gyrus	6
			L-frontal	4.00	−7, 11, 66	Superior frontal gyrus	6
			L-parietal	3.91	−46, −26, 29	Postcentral gyrus	2
			R-frontal	3.64	42, 9, 59	Middle frontal gyrus	6

Uncorrected $p < 0.001$ at peak level and $p < 0.05$, false discovery rate corrected at cluster level, were accepted as statistically significant. In the "cluster level" section on the left, for each cluster found to be statistically significant, the number of voxels, the corrected p value and the cortical region where the cluster is found are reported. In the "peak level" section on the right, for each significant cluster, the peak coordinates and Z score, the corresponding cortical region and Brodmann area (BA) are reported. L, left; R, right.

caudate connections, are interestingly missed in the patient group. It is known that the caudate nucleus is highly involved in functions such as learning and memory (Graybiel, 2005; Jokinen et al., 2009) whose impairment is a hallmark of AD.

Neocortical functional changes have been demonstrated in AD using fMRI, including decreased activation in prefrontal regions. A quantitative meta-analysis (Schwindt and Black, 2009) of both fMRI and FDG-PET memory activation studies in AD identified several regions, including ventrolateral prefrontal cortex as the ones more likely to show greater encoding-related activation in controls than in AD patients. Moreover, impaired prefrontal lobe function and a trend toward reduced hippocampal activity were observed in mild AD (Greicius et al., 2004).

Small clusters of correlation in right temporal and parietal cortex were found in the pAD group when analyzing resting metabolic connectivity of right DLFC. This may well be the result of chance. Alternatively, because the right hemisphere was relatively less affected in the pAD group (see Fig. 1), it might be the result of residual compensatory mechanisms. Some studies reported increased frontal-parietal functional connections in aMCI patients that are still trying to compensate the lack of other functional connections (Guedj et al., 2009; Qi et al., 2010). When patients were divided into APOE ε4+ and APOE ε4− subgroups, these small clusters were confirmed in APOE ε4− but not in APOE ε4+ subgroup (Supplementary data). The presence of frontoparietal compensation in APOE ε4− but not in APOE ε4+ patients is in keeping with the reported higher associative cortex damage (hypometabolism) in APOE ε4+ carriers compared with the general AD population (During et al., 2011; Mosconi et al., 2004a; Reiman et al., 2001).

Finally, the findings of preserved metabolic connectivity in bilateral SM in the pAD group is in agreement with the neuropathology and imaging-derived concept that sensorimotor area is substantially spared in the preclinical phase of AD (Braak and Braak, 1996; Whitwell et al., 2007).

It should be underlined that the lack of information about APOE genotype in a part of patients, the inclusion of normal subjects acquired in a single center in the normalization template, and the use of different PET scanners are all potential limitations of this study. However, the last inhomogeneity was taken into account by a multiple approach, including the balanced number of patients and controls among centers and the covariation for the recording center as a "nuisance" variable in all SPM analyses.

4.1. Conclusions

In summary, the present findings give support to the hypothesis that AD patients have widespread disturbance in functional connectivity already in the prodromal stage.

The pathophysiological process of AD seems to be associated with alterations in large-scale functional brain networks, in particular, the DMN and networks supporting memory function. The combination of activation studies and resting functional connectivity studies should provide further insight into the link between pathology and brain function in AD. Further studies are needed to ascertain whether resting functional connectivity studies can be used on an individual basis to predict cognitive decline, conversion, or even response to disease-modifying therapy in the preclinical phases of AD.

Disclosure statement

The authors disclose no conflicts of interest.

The study was approved by the local Medical Ethics Committee in each center and all the recruited subjects provided written informed consent.

Appendix A. Supplementary data

Supplementary data associated with this article can be found, in the online version, at doi:10.1016/j.neurobiolaging.2012.01.005.

References

Azari, N.P., Rapoport, S.I., Grady, C.L., Schapiro, M.B., Salerno, J.A., Gonzalez-Aviles, A., Horwitz, B., 1992. Patterns of interregional correlations of cerebral glucose metabolic rates in patients with dementia of the Alzheimer type. Neurodegeneration 1, 45–54.

Bartenstein, P., Asenbaum, S., Catafau, A., Halldin, C., Pilowski, L., Pupi, A., Tatsch, K., 2002. European Association of Nuclear Medicine procedure guidelines for brain imaging using [(18)F]FDG. Eur. J. Nucl. Med. 29, BP43–BP48.

Beason-Held, L.L., Kraut, M.A., Resnick, S.M., 2009. Stability of default-mode network activity in the aging brain. Brain Imaging Behav. 14, 123–131.

Biswal, B., Yetkin, F.Z., Haughton, V.M., Hyde, J.S., 1995. Functional connectivity in the motor cortex of resting human brain using echo-planar MRI. Magn. Reson. Med. 34, 537–541.

Bookheimer, S.Y., Strojwas, M.H., Cohen, M.S., Saunders, A.M., Pericak-Vance, M.A., Mazziotta, J.C., Small, G.W., 2000. Patterns of brain activation in people at risk for Alzheimer's disease. N. Engl. J. Med. 343, 450–456.

Braak, H., Braak, E., 1996. Evolution of the neuropathology of Alzheimer's disease. Acta Neurol. Scand. Suppl. 165, 3–12.

Bressler, S.L., Menon, V., 2010. Large-scale brain networks in cognition: emerging methods and principles. Trends Cogn. Sci. 14, 277–290.

Buckner, R.L., Andrews-Hanna, J.R., Schacter, D.L., 2008. The brain's default network. Anatomy, function and relevance to disease. Ann. N. Y. Acad. Sci. 1124, 1–38.

Damoiseaux, J.S., Rombouts, S.A., Barkhof, F., Scheltens, P., Stam, C.J., Smith, S.M., Beckmann, C.F., 2006. Consistent resting-state networks across healthy subjects. Proc. Natl. Acad. Sci. U. S. A. 103, 13848–13853.

de Leon, M.J., Ferris, S.H., George, A.E., Reisberg, B., Christman, D.R., Kricheff, I.I., Wolf, A.P., 1983. Computed tomography and positron emission transaxial tomography evaluations of normal aging and Alzheimer's disease. J. Cereb. Blood Flow Metab. 3, 391–394.

Dickerson, B.C., Sperling, R.A., 2009. Large-scale functional brain network abnormalities in Alzheimer's disease: insights from functional neuroimaging. Behav. Neurol. 21, 63–75.

Drzezga, A., Becker, J.A., Van Dijk, K.R., Sreenivasan, A., Talukdar, T., Sullivan, C., Schultz, A.P., Sepulcre, J., Putcha, D., Greve, D., Johnson, K.A., Sperling, R.A., 2011. Neuronal dysfunction and disconnection of cortical hubs in non-demented subjects with elevated amyloid burden. Brain 134, 1635–1646.

Drzezga, A., Grimmer, T., Peller, M., Wermke, M., Siebner, H., Rauschecker, J.P., Schwaiger, M., Kurz, A., 2005. Impaired cross-modal inhibition in Alzheimer disease. PLoS Med. 2, 288.

During, E.H., Osorio, R.S., Elahi, F.M., Mosconi, L., de Leon, M.J., 2011. The concept of FDG-PET endophenotype in Alzheimer's disease. Neurol. Sci. 32, 559–569.

Friston, K.J., Holmes, A.P., Worsley, K.J., Poline, J.P., Frith, C.D., Frackowiak, R.S.J., 1994. Statistical parametric maps in functional imaging: a general linear approach. Hum. Brain Mapp. 2, 189–210.

Gispert, J.D., Pascau, J., Reig, S., Martínez-Lázaro, R., Molina, V., García-Barreno, P., Desco, M., 2003. Influence of the normalization template on the outcome of statistical parametric mapping of PET scans. Neuroimage 19, 601–612.

Graybiel, A.M., 2005. The basal ganglia: learning new tricks and loving it. Curr. Opin. Neurobiol. 15, 638–644.

Greicius, M.D., Srivastava, G., Reiss, A.L., Menon, V., 2004. Default-mode network activity distinguishes Alzheimer's disease from healthy aging: evidence from functional MRI. Proc. Natl. Acad. Sci. U. S. A. 30, 4637–4642.

Gruetter, R., Adriany, G., Choi, I.Y., Henry, P.G., Lei, H., Oz, G., 2003. Localized in vivo 13C NMR spectroscopy of the brain. NMR Biomed. 16, 313–338.

Guedj, E., Barbeau, E.J., Didic, M., Felician, O., de Laforte, C., Ranjeva, J.P., Poncet, M., Cozzone, P.J., Mundler, O., Ceccaldi, M., 2009. Effects of medial temporal lobe degeneration on brain perfusion in amnestic MCI of AD type: deafferentation and functional compensation? Eur. J. Nucl. Med. Mol. Imaging 36, 1101–1112.

Horwitz, B., Duara, R., Rapoport, S.I., 1984. Intercorrelations of glucose metabolic rates between brain regions: application to healthy males in a state of reduced sensory input. J. Cereb. Blood Flow Metab. 4, 484–499.

Horwitz, B., Grady, C.L., Schlageter, N.L., Duara, R., Rapoport, S.I., 1987. Intercorrelations of regional cerebral glucose metabolic rates in Alzheimer's disease. Brain Res. 407, 294–306.

Horwitz, B., Rumsey, J.M., Grady, C.L., Rapoport, S.I., 1988. The cerebral metabolic landscape in autism. Intercorrelations of regional glucose utilization. Arch. Neurol. 45, 749–755.

Horwitz, B., Schapiro, M.B., Grady, C.L., Rapoport, S.I., 1990. Cerebral metabolic pattern in young adult Down's syndrome subjects: altered intercorrelations between regional rates of glucose utilization. J. Ment. Defic. Res. 34, 237–252.

Horwitz, B., Swedo, S.E., Grady, C.L., Pietrini, P., Schapiro, M.B., Rapoport, J.L., Rapoport, S.I., 1991. Cerebral metabolic pattern in obsessive-compulsive disorder: altered intercorrelations between regional rates of glucose utilization. Psychiatry Res. 40, 221–237.

Huang, S., Li, J., Sun, L., Ye, J., Fleisher, A., Wu, T., Chen, K., Reiman, E., 2010. Alzheimer'sDisease NeuroImaging Initiative. Learning brain connectivity of Alzheimer's disease by sparse inverse covariance estimation. Neuroimage 15, 935–949.

Hughes, C.P., Berg, L., Danziger, W.L., Coben, L.A., Martin, R.L., 1982. A new clinical scale for the staging of dementia. Br. J. Psychiatry 140, 566–572.

Hyder, F., Patel, A.B., Gjedde, A., Rothman, D.L., Behar, K.L., Shulman, R.G., 2006. Neuronal-glial glucose oxidation and glutamatergic–GABAergic function. J. Cereb. Blood Flow Metab. 26, 865–877.

Hyman, B.T., Van Hoesen, G.W., Damasio, A.R., Barnes, C.L., 1984. Alzheimer's disease: cell-specific pathology isolates the hippocampal formation. Science 225, 1168–1170.

Jokinen, P., Bruck, A., Aalto, S., Forsback, S., Parkkola, R., Rinne, J.O., 2009. Impaired cognitive performance in Parkinson's disease is related to caudate dopaminergic hypofunction and hippocampal atrophy. Parkinsonism Relat. Disord. 15, 88–93.

Kahn, I., Andrews-Hanna, J.R., Vincent, J.L., Snyder, A.Z., Buckner, R.L., 2008. Distinct cortical anatomy linked to subregions of the medial temporal lobe revealed by intrinsic functional connectivity. J. Neurophysiol. 100, 129–139.

Kang, E., Lee, D.S., Lee, J.S., Kang, H., Hwang, C.H., Oh, S.H., Kim, C.S., Chung, J.K., Lee, M.C., Jang, M.J., Lee, Y.J., Morosan, P., Zilles, K., 2003. Developmental hemispheric asymmetry of interregional metabolic correlation of the auditory cortex in deaf subjects. Neuroimage 19, 777–783.

Kas, A., Payoux, P., Habert, M.O., Malek, Z., Cointepas, Y., El Fakhri, G., Chaumet-Riffaud, P., Itti, E., Remy, P., 2007. Validation of a standardized normalization template for statistical parametric mapping analysis of 123I-FP-CIT images. J. Nucl. Med. 48, 1459–1467.

Lacor, P.N., Buniel, M.C., Furlow, P.W., Clemente, A.S., Velasco, P.T., Wood, M., Viola, K.L., Klein, W.L., 2007. Abeta oligomer-induced aberrations in synapse composition, shape, and density provide a molecular basis for loss of connectivity in Alzheimer's disease. J. Neurosci. 27, 796–807.

Lee, D.S., Kang, H., Kim, H., Park, H., Oh, J.S., Lee, J.S., Lee, M.C., 2008. Metabolic connectivity by interregional correlation analysis using statistical parametric mapping (SPM) and FDG brain PET; methodological development and patterns of metabolic connectivity in adults. Eur. J. Nucl. Med. Mol. Imaging 35, 1681–1691.

Lustig, C., Snyder, A.Z., Bhakta, M., O'Brien, K.C., McAvoy, M., Raichle, M.E., Morris, J.C., Buckner, R.L., 2003. Functional deactivations: change with age and dementia of the Alzheimer type. Proc. Natl. Acad. Sci. U. S. A. 100, 14504–14509.

Magistretti, P.J., Pellerin, L., 1999. Cellular mechanisms of brain energy metabolism and their relevance to functional brain imaging. Philos. Trans. R. Soc. Lond. B Biol. Sci. 354, 1155–1163.

Maldjian, J.A., Laurienti, P.J., Kraft, R.A., Burdette, J.H., 2003. An Automated Method for Neuroanatomic and Cytoarchitectonic Atlas-based Interrogation of fMRI Data Sets. Neuroimage 19, 1233–1239.

McKhann, G., Drachman, D., Folstein, M., Katzman, R., Price, D., Stadlan, E.M., 1984. Clinical diagnosis of Alzheimer's disease: report of the NINCDS-ADRDA Work Group under the auspices of Department of Health and Human Services Task Force on Alzheimer's Disease. Neurology 34, 939–944.

Meguro, K., Blaizot, X., Kondoh, Y., Le Mestric, C., Baron, J.C., Chavoix, C., 1999. Neocortical and hippocampal glucose hypometabolism following neurotoxic lesions of the entorhinal and perirhinal cortices in the non-human primate as shown by PET. Implications for Alzheimer's disease. Brain 122, 1519–1531.

Meyer, J.H., Gunn, R.N., Myers, R., Grasby, P.M., 1999. Assessment of spatial normalization of PET ligand images using ligand-specific templates. Neuroimage 9, 545–553.

Minoshima, S., Giordani, B., Berent, S., Frey, K.A., Foster, N.L., Kuhl, D.E., 1997. Metabolic reduction in the posterior cingulate cortex in very early Alzheimer's disease. Ann. Neurol. 42, 85–94.

Morbelli, S., Piccardo, A., Villavecchia, G., Dessi, B., Brugnolo, A., Piccini, A., Caroli, A., Frisoni, G., Rodriguez, G., Nobili, F., 2010. Mapping brain morphological and functional conversion patterns in amnestic MCI: a voxel-based MRI and FDG-PET study. Eur. J. Nucl. Med. Mol. Imaging 37, 36–45.

Mosconi, L., 2005. Brain glucose metabolism in the early and specific diagnosis of Alzheimer's disease. FDG-PET studies in MCI and AD. Eur. J. Nucl. Med. Mol. Imaging 32, 486–510.

Mosconi, L., Nacmias, B., Sorbi, S., De Cristofaro, M.T., Fayazz, M., Tedde, A., Bracco, L., Herholz, K., Pupi, A., 2004a. Brain metabolic decreases related to the dose of the ApoE e4 allele in Alzheimer's disease. J. Neurol. Neurosurg. Psychiatry 75, 370–376.

Mosconi, L., Perani, D., Sorbi, S., Herholz, K., Nacmias, B., Holthoff, V., Salmon, E., Baron, J.C., De Cristofaro, M.T., Padovani, A., Borroni, B., Franceschi, M., Bracco, L., Pupi, A., 2004c. MCI conversion to

dementia and the APOE genotype: a prediction study with FDG-PET. Neurology 63, 2332–2340.

Mosconi, L., Pupi, A., De Cristofaro, M.T., Fayyaz, M., Sorbi, S., Herholz, K., 2004b. Functional interactions of the entorhinal cortex: an 18F-FDG PET study on normal aging and Alzheimer's disease. J. Nucl. Med. 45, 382–392.

Nestor, P.J., Scheltens, P., Hodges, J.R., 2004. Advances in the early detection of Alzheimer's disease. Nat. Med. 10, S34–S41.

Nobili, F., Salmaso, D., Morbelli, S., Girtler, N., Piccardo, A., Brugnolo, A., Dessi, B., Larsson, S.A., Rodriguez, G., Pagani, M., 2008. Principal component analysis of FDG PET in amnestic MCI. Eur. J. Nucl. Med. Mol. Imaging 35, 2191–2202.

Oishi, N., Udaka, F., Kameyama, M., Sawamoto, N., Hashikawa, K., Fukuyama, H., 2005. Regional cerebral blood flow in Parkinson disease with nonpsychotic visual hallucinations. Neurology 65, 1708–1715.

Petersen, R.C., 2004. Mild cognitive impairment as a diagnostic entity. J. Intern. Med. 256, 183–194.

Price, J.L., Morris, J.C., 1999. Tangles and plaques in nondemented aging and "preclinical" Alzheimer's disease. Ann. Neurol. 45, 358–368.

Qi, Z., Wu, X., Wang, Z., Zhang, N., Dong, H., Yao, L., Li, K., 2010. Impairment and compensation coexist in amnestic MCI default mode network. Neuroimage 50, 48–55.

Raichle, M.E., MacLeod, A.M., Snyder, A.Z., Powers, W.J., Gusnard, D.A., Shulman, G.L., 2001. A default mode of brain function. Proc. Natl. Acad. Sci. U. S. A. 16, 676–682.

Reiman, E.M., Caselli, R.J., Chen, K., Alexander, G.E., Bandy, D., Frost, J., 2001. Declining brain activity in cognitively normal apolipoprotein E epsilon 4 heterozygotes: a foundation for using positron emission tomography to efficiently test treatments to prevent Alzheimer's disease. Proc. Natl. Acad. Sci. U. S. A. 98, 3334–3339.

Rosario, B.L., Ziolko, S.K., Weissfeld, L.A., Price, J.C., 2008. Assessment of parameter settings for SPM5 spatial normalization of structural MRI data: application to type 2 diabetes. Neuroimage 41, 363–370.

Salmon, E., Kerrouche, N., Perani, D., Lekeu, F., Holthoff, V., Beuthien-Baumann, B., Sorbi, S., Lemaire, C., Collette, F., Herholz, K., 2009. On the multivariate nature of brain metabolic impairment in Alzheimer's disease. Neurobiol. Aging 30, 186–197.

Schwindt, G.C., Black, S.E., 2009. Functional imaging studies of episodic memory in Alzheimer's disease: a quantitative meta-analysis. Neuroimage 45, 181–190.

Sestini, S., Castagnoli, A., Mansi, L., 2010. The new FDG brain revolution: the neurovascular unit and the default network. Eur. J. Nucl. Med. Mol. Imaging 37, 913–916.

Vincent, J.L., Snyder, A.Z., Fox, M.D., Shannon, B.J., Andrews, J.R., Raichle, M.E., Buckner, R.L., 2006. Coherent spontaneous activity identifies a hippocampal-parietal memory network. J. Neurophysiol. 96, 3517–3531.

Vogt, B.A., Vogt, L., Laureys, S., 2006. Cytology and functionally correlated circuits of human posterior cingulate areas. Neuroimage 29, 452–466.

Whitwell, J.L., Przybelski, S.A., Weigand, S.D., Knopman, D.S., Boeve, B.F., Petersen, R.C., Jack, C.R., 2007. 3D maps from multiple MRI illustrate changing atrophy patterns as subjects progress from mild cognitive impairment to Alzheimer's disease. Brain 130, 1777–1786.

Zelazo, P.D., Muller, U., 2002. Executive function in typical and atypical development, in: Goswam, U. (Ed.), Blackwell Handbook of Child Cognitive Development. Oxford, UK, Blackwell Publishers Ltd; Chapter 20; pp. 445–469.